ChemComm

COMMUNICATION

View Article Online
View Journal | View Issue

Cite this: *Chem. Commun.*, 2019, **55**, 8780

Received 25th February 2019,
Accepted 25th March 2019

DOI: 10.1039/c9cc01585j

rsc.li/chemcomm

Tunneling and thermoelectric characteristics of N-heterocyclic carbene-based large-area molecular junctions†

Seohyun Kang, Sohyun Park, Hungu Kang, Soo Jin Cho, Hyunsun Song and Hyo Jae Yoon *

Reported herein are tunneling and thermoelectric characteristics of large-area molecular junctions formed with N-heterocyclic carbene (NHC)-based self-assembled monolayers on gold.

Large-area molecular junctions formed with self-assembled monolayers (SAMs) formed *via* thiol chemistry over coinage metal substrates have been widely harnessed in the study of organic and molecular electronics.[1–3] Indeed, molecular junctions incorporating thiol-based SAMs have shown their utility in fundamental understanding of molecular conduction[4–11] and various applications including molecular diodes,[12–17] photo-switches,[18,19] negative differential resistors,[20] thermoelectrics,[21–23] and plasmonics.[24] However, as free thiols and thiolates anchored on a substrate can be easily oxidized and decomposed by oxygen in the air and photoirradiation,[25–27] thiol-based SAMs often do not guarantee long-term stability and durability.[25] To circumvent this problem, Crudden *et al.*[28] have reported a stimulating work in 2014 that utilizes the N-heterocyclic carbene (NHC) chemistry over gold to form thiol-free, robust SAMs not only under ambient conditions but also under high temperature and chemically/electrochemically active conditions. In 2018, Doud *et al.*[29] reported the first NHC-based single-molecule junction *via* incorporation of MeS(Ph)$_n$NHC–MCl complexes (M = Au, Ag, and Cu; n = 0, 1, and 2) into scanning tunneling microscope-based break junction (STM-BJ). According to this previous work, the conductance depends on the metal in the precursor (decreasing in the order of M = Au > Ag > Cu). It has been noted that the junctions formed with solutions of free NHCs did not yield reproducible conductance results.

Herein, we show for the first-time fabrication of large-area molecular junctions of NHC-based monolayers constructed directly from solutions of metal-free NHC derivatives and examine their tunneling and thermoelectric characteristics.

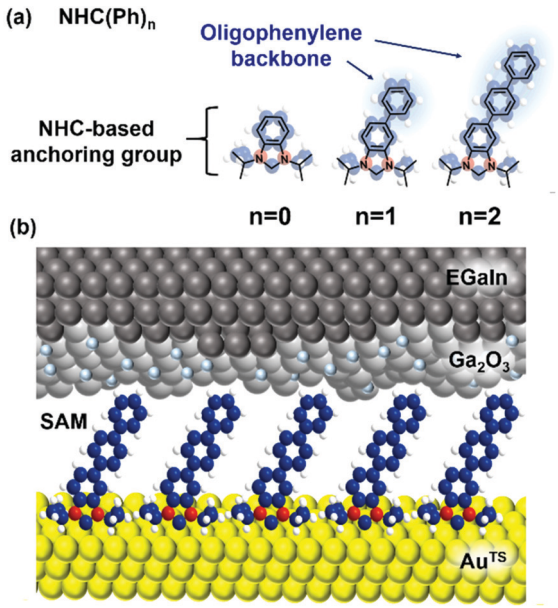

Fig. 1 (a) Molecules used in this study. (b) A schematic describing the structure of the large-area molecular junction we used.

Oligophenylene-NHC SAMs (denoted as NHC(Ph)$_n$ where n = 0, 1, and 2; Fig. 1a) were formed on ultraflat template-stripped gold (Au^{TS}),[30] and electrically and thermoelectrically characterized with a liquid metal top-electrode comprising eutectic Ga–In alloy (EGaIn)[21,31] covered with a conductive native oxide of ~1 nm nominal thickness (Fig. 1b). We observed the length dependence of tunneling current density (J, A cm^{-2}) across the junctions, obeying a rectangular energy barrier model, the simplified Simmons model.[5,32] Junction measurements at low temperatures indicate the charge transport across the NHC-based large-area junctions occurring in a pure tunneling regime, not relying on a thermal hopping process. Thermoelectric characterization over identical junctions showed that thermopower increased with increasing length of the molecule. The positive sign of the measured Seebeck coefficient values implies that the frontier

Department of Chemistry, Korea University, Seoul, 02841, South Korea.
E-mail: hyoon@korea.ac.kr

† Electronic supplementary information (ESI) available: Experimental procedures and further discussions. See DOI: 10.1039/c9cc01585j

molecular orbital close to the Fermi level of the electrode is the highest occupied molecular orbital (HOMO) rather than the lowest unoccupied molecular orbital (LUMO), and the molecular conduction is dominated by hole tunneling.

We synthesized NHC(Ph)$_n$ hydrogen carbonate salts (NHC(Ph)$_n$-HCO_3) as NHC precursors,[33] following the synthetic schemes presented in Scheme S1 in the ESI.† The ^{1}H and ^{13}C NMR spectroscopic analyses and the high resolution mass spectrometric analysis confirmed the desired structures (see the ESI† for details). To form NHC SAMs on Au^{TS}, a freshly prepared Au^{TS} chip was placed in an ethanolic solution of 2 mM NHC(Ph)$_n$$HCO_3$.[33] After 3 h incubation at room temperature in the air, the resulting SAM-bound Au^{TS} chip was rinsed with pure ethanol and dried in air (see the ESI† for details). The Au^{TS}/NHC(Ph)$_n$ SAMs were characterized with X-ray photoelectron spectroscopy (XPS), and static and dynamic contact angle goniometries. The XPS spectra (Fig. S6–S8 in the ESI†) exhibited the presence of nitrogen, carbon and oxygen atoms in all the SAMs. A single binding energy of N1s was observed at 402.5 eV; the C1s peak was deconvoluted into three signals, which corresponded to C–O, C–N, and C–C/C=C, respectively.[28,29,34] As the number of phenylene units increased, the intensity ratio of C–C/C=C to C–N signals increased (Table S3 in the ESI†). XPS data showed that all the SAMs have oxygen atoms, and the peak of O1s was observed at 525 eV. This is attributed to the decomposition by-products (CO_2 and/or H_2O formed upon chemisorption of the NHC precursor) trapped in the monolayers on the substrates.[28,33,34] As shown in Fig. S12 in the ESI,† the static contact angle (θ_s) and the dynamic contact angle ($\Delta\cos\theta_d$: the difference in advancing ($\cos\theta_a$) and receding ($\cos\theta_r$) contact angles) did not significantly change with the increasing length (n in NHC(Ph)$_n$). These observations indicate that all the SAMs have similar surface energy and roughness regardless of the number of phenylene units.

The electronic structure of the NHC(Ph)$_n$ SAMs was characterized using ultraviolet photoelectron spectroscopy (UPS) and Kelvin probe force microscopy (KPFM) (Fig. S12 in the ESI†). From the UPS and KPFM studies, the work function (WF) of the Au^{TS}/NHC(Ph)$_n$ SAMs was estimated through measurements of secondary electron cutoff (SECO) and contact potential difference (CPD), respectively (see the ESI† for details). The UPS-based WF values ranged from 3.45–4.04 eV, similar to the previous observation.[35] The trends of WF estimated by UPS and KPFM were similar although there were some deviations between the absolute values. Values of KPFM-based WF were obtained by relative comparison of target samples with the WF ($\sim$4.5 eV) of highly oriented pyrolytic graphite (HOPG). We did not observe the correlation between the WF and the molecular length.

To measure $J(V)$ across junctions, we formed junctions with a cone-shaped EGaIn microelectrode following the previously reported methods.[11,31,36] The EGaIn microelectrode permits noninvasive and reversible top-contacts over SAMs. We obtained 374–468 J–V traces from 20–27 separate junctions in six different samples for each molecule. Values of J across Au^{TS}/NHC-(Ph)$_n$//Ga_2O_3/EGaIn junctions at $\pm$1.0 V were log-normally distributed (Fig. 2a). The degree of asymmetric feature in the J–V curve is quantitatively defined as rectification: $|r^+| = |J(+V)|/|J(-V)|$.

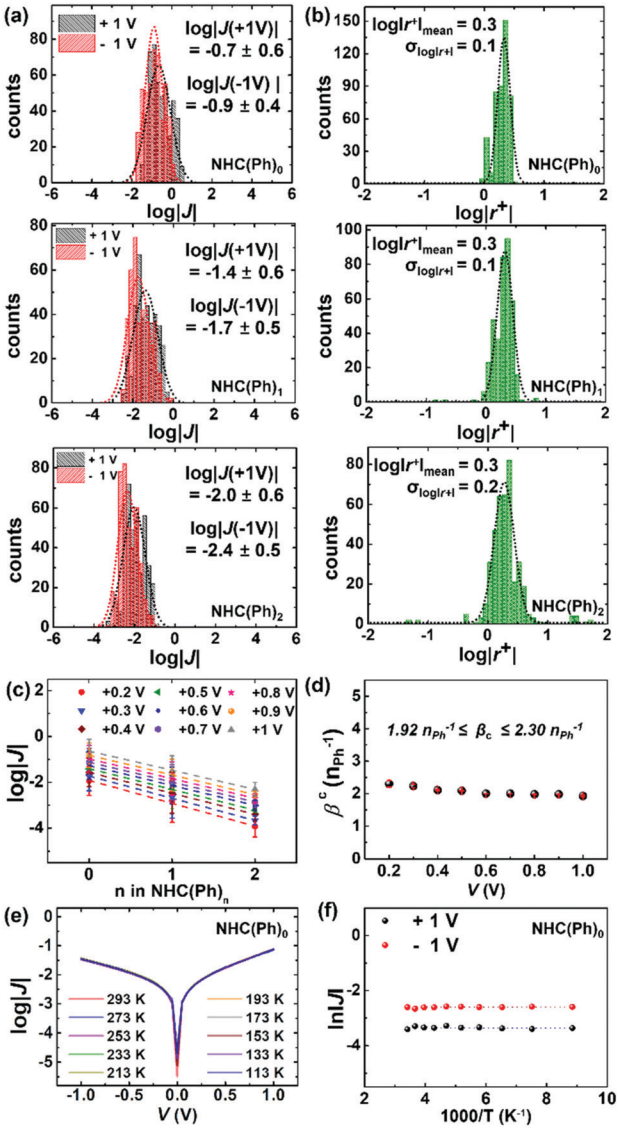

Fig. 2 Histograms of (a) log|J| and (b) log|r^+| at $\pm$1.0 V for NHC(Ph)$_n$ (n = 0, 1, and 2) SAM. (c) Linear correlation between the log|J| and the molecular length. (d) Constant β^c value regardless of applied voltage. (e) Exemplary log|J|–V traces measured at low temperatures (from 113 to 293 K) for Au^{TS}/NHC(Ph)$_0$//Ga_2O_3/EGaIn junctions. (f) The corresponding Arrhenius plots.

The SAMs showed modest rectification ratios ($1.9 < |r^+| < 2.1$ at $\pm$1.0 V; Fig. 2b), similar to the rectification ratios observed in conventional n-alkane and oligophenylene thiolates.[5,37] Mean (log|J|$_{mean}$), median (log|J|$_{median}$) and standard deviation ($\sigma_{log|J|}$) were extracted from fitting of log|J| histograms with single Gaussian curves. Table S1 in the ESI† summarizes the data of junction measurements. The yield of working junctions ranged from 88 to 92%. Fig. 2c shows that log|J| linearly decreased with the increasing length of the molecule. This linear regression indicates that the tunneling current density across junctions well-obeys the simplified Simmons model (eqn (1)):[5,6,32]

$$J = J_0 \times \exp(-\beta^c d) \quad (1)$$

Here, J_0 is the tunneling injection current (A cm^{-2}), β^c is the tunneling decay coefficient (here, per phenylene; n_{Ph}^{-1}), and d is the width of the tunneling barrier, usually taken from the length of the molecule. We estimated the values of β^c and J_0 from the slope and y-intercept in the plot of $\log|J|_{mean}$ against the number of phenylene units (Fig. 2c): at +1.0 V, $\beta^c = 1.93 \pm 0.02$ n_{Ph}^{-1} and $J_0 = -0.64 \pm 0.02$ A cm^{-2}. The linear correlation between the $\log|J|$ and the molecular length was retained in different voltages (Fig. 2d). Our value of β^c (1.93 ± 0.02 n_{Ph}^{-1}) was similar to that (2.4 ± 0.1 n_{Ph}^{-1}) of an analogous junction ($Ag^{TS}/O_2C(Ph)_n//Ga_2O_3/EGaIn$) containing a different anchoring group (carboxylate),[37] and that (1.7 ± 0.1 n_{Ph}^{-1}) of a different junction ($Au/NH_2(Ph)_nNH_2/Au$).[38] To determine if the transport across our junctions depends on the thermal hopping process or not, we formed the analogous EGaIn junction in an untethered form, following the previously reported procedure.[39] The J value did not significantly vary with lowering the temperature up to ~110 K (Fig. 2e and f), indicating that pure tunneling dominates the charge transport in the NHC-based large-area junctions.

With the identical junction architecture, we measured for the first time the Seebeck coefficient of the NHC-based monolayers (Fig. 3a), following the previously reported procedures.[21] Briefly, a SAM-bound Au^{TS} chip was placed on a hot chuck, and exposed to a finite temperature. A microelectrode comprising EGaIn was then brought onto the SAM, and the thermoelectric voltage (ΔV) created by the temperature differential (ΔT) applied to the junction was measured (see the ESI† for details). We measured ΔV values for ΔT = 2, 4 and 6 K (Fig. 3b). Overall, the distribution of ΔV was broadened as the value of ΔT and the number of phenylene units were increased, as shown in ΔV histograms (Fig. S13 in the ESI†). This observation was consistent with the results observed in other thermoelectric junctions.[21,40,41] The increased ΔT and the structural complexity of the molecule induce an increase in the degree of freedom (by variation in C–C torsional angles) and internal vibration, thereby leading to largely dispersed data of ΔV.[41] The Seebeck coefficient (S, μV K^{-1}; $S = -\Delta V/\Delta T$) of the SAM (S_{SAM}) was extracted through the thermopower analysis of the circuit equivalent to the junction (Fig. S5 in the ESI†). Finally, using the following equation, we obtained the S_{SAM} values:

$$\Delta V = -(S_{SAM} - S_{W\,tip}) \times \Delta T \quad (2)$$

The data of thermopower measurements are summarized in Table S2 in the ESI.† All the NHC(Ph)$_n$ junctions exhibited positive values of S_{SAM} (Table S2, ESI†). This indicates that the transport in our junctions is dominated by the HOMO, not the LUMO. Our finding is against the previous calculation[29] that shows that the LUMO is close to the E_F of the electrode in the NHC-based single molecule junction. This discrepancy can be explained by the different top-interfaces: our junction has the van der Waals top-contact whereas the junction in the previous work does not. The thermopower in the NHC-based junctions was further investigated by transmission function-based modelling (see the ESI† for details).[22,42] As shown in Fig. 3c, the experimentally observed length dependence and sign of S_{SAM} were reproduced, at least qualitatively, by the modelling (Fig. 3d). There were some deviations between experimental and calculated values, which could be attributed to complexities arising from the top-contact and the molecular vibrations that are not reflected in the modelling.[22]

The linear correlation between the S_{SAM} and the molecular length can be explained by a simplified model (eqn (3)) proposed

$$S_{SAM} = S_C + n \cdot \beta^S \quad (3)$$

by Quek *et al.*[43] Here, S_C is the thermopower of a hypothetical non-shorting junction that does not contain the insulating molecular component; n is the number of phenylene units; and β^S is the change rate of thermopower. The y-intercept and slope in the plot of Fig. 3d corresponded to S_C and β^S, respectively. The value of β^S (2.1 ± 0.4 μV (K n_{Ph})$^{-1}$) for the NHC-based junctions was statistically indistinguishable from those of oligophenylene monothiolates (2.1 ± 0.3 μV (K n_{Ph})$^{-1}$)[21] and dithiolates (2.8 ± 0.8 μV (K n_{Ph})$^{-1}$)[40] measured in different junction testbeds. On the other hand, there was a noticeable difference in S_C among the junctions: the value of S_C (8.2 ± 0.8 μV K^{-1}) for the NHC-based junctions was smaller than those of oligophenylene monothiolates (5.6 ± 0.5 μV K^{-1})[21] and dithiolates (6.4 ± 1.8 μV K^{-1}),[40] respectively. This difference could be explained by the thermopower difference between the different anchoring moieties (thiolate *vs.* NHC). The S_C value corresponds to the sum of thermopowers of NHC ($S_{Au\text{-}NHC}$) and van der Waals (S_{vdW}) contacts. Similarly, the value of S_{vdW} could be obtained from the previous work involving oligophenylene monothiolates:[21] S_{vdW} = 2.4 μV K^{-1}. Thus, the value of $S_{Au\text{-}NHC}$ was estimated as $S_C - S_{vdW}$ = 5.8 μV K^{-1}.

In conclusion, we have investigated for the first-time tunneling and thermoelectric properties of NHC-based large-area junctions through a combined experimental and computational approach. Our studies indicate that the charge tunneling of NHC-based

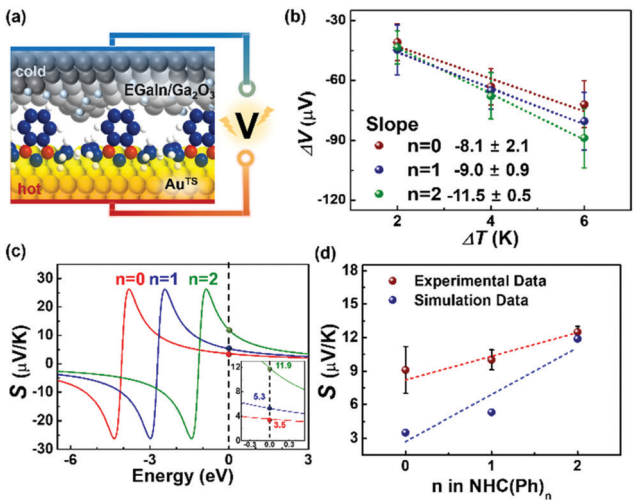

Fig. 3 (a) A schematic describing the structure of the large-area thermoelectric junction. (b) Plots of ΔV as a function of ΔT. (c) Simulations of S values based on the transmission function and Landauer formula (eqn (S2) and (S3) in the ESI†). The inset shows the magnification of Seebeck coefficient near the Fermi level of EGaIn. (d) Plots of experimental and theoretical S values as a function of the molecular length.

monolayers follows the Simmons model widely used for studies of molecular conduction, and the Seebeck coefficient is positive in sign and increases with molecular length. Our computational studies confirm these empirical findings.

This research was supported by the NRF of Korea (NRF-2017M3A7B8064518).

Conflicts of interest

There are no conflicts to declare.

Notes and references

1 A. Vilan, D. Aswal and D. Cahen, *Chem. Rev.*, 2017, **117**, 4248.
2 D. Xiang, X. L. Wang, C. C. Jia, T. Lee and X. F. Guo, *Chem. Rev.*, 2016, **116**, 4318.
3 J. C. Love, L. A. Estroff, J. K. Kriebel, R. G. Nuzzo and G. M. Whitesides, *Chem. Rev.*, 2005, **105**, 1103–1169.
4 H. J. Yoon, N. D. Shapiro, K. M. Park, M. M. Thuo, S. Soh and G. M. Whitesides, *Angew. Chem., Int. Ed.*, 2012, **51**, 4658.
5 F. C. Simeone, H. J. Yoon, M. M. Thuo, J. R. Barber, B. Smith and G. M. Whitesides, *J. Am. Chem. Soc.*, 2013, **135**, 18131.
6 H. J. Yoon, C. M. Bowers, M. Baghbanzadeh and G. M. Whitesides, *J. Am. Chem. Soc.*, 2014, **136**, 16.
7 J. Chen, M. Kim, S. Gathiaka, S. J. Cho, S. Kundu, H. J. Yoon and M. M. Thuo, *J. Phys. Chem. Lett.*, 2018, **9**, 5078.
8 J. Jin, G. D. Kong and H. J. Yoon, *J. Phys. Chem. Lett.*, 2018, **9**, 4578.
9 Z. Xie, I. Bâldea and C. D. Frisbie, *Chem. Sci.*, 2018, **9**, 4456.
10 J. M. Beebe, B. Kim, C. D. Frisbie and J. G. Kushmerick, *ACS Nano*, 2008, **2**, 827.
11 G. D. Kong, J. Jin, M. M. Thuo, H. Song, J. F. Joung, S. Park and H. J. Yoon, *J. Am. Chem. Soc.*, 2018, **140**, 12303.
12 N. Nerngchamnong, L. Yuan, D. C. Qi, J. Li, D. Thompson and C. A. Nijhuis, *Nat. Nanotechnol.*, 2013, **8**, 113.
13 H. J. Yoon, K. C. Liao, M. R. Lockett, S. W. Kwok, M. Baghbanzadeh and G. M. Whitesides, *J. Am. Chem. Soc.*, 2014, **136**, 17155.
14 L. Qiu, Y. X. Zhang, T. L. Krijger, X. K. Qiu, P. van't Hof, J. C. Hummelen and R. C. Chiechi, *Chem. Sci.*, 2017, **8**, 2365.
15 S. J. Cho, G. D. Kong, S. Park, J. Park, S. E. Byeon, T. Kim and H. J. Yoon, *Nano Lett.*, 2019, **19**, 545.
16 G. J. Ashwell and A. Mohib, *J. Am. Chem. Soc.*, 2005, **127**, 16238.
17 M. L. Chabinyc, X. X. Chen, R. E. Holmlin, H. Jacobs, H. Skulason, C. D. Frisbie, V. Mujica, M. A. Ratner, M. A. Rampi and G. M. Whitesides, *J. Am. Chem. Soc.*, 2002, **124**, 11730.
18 C. C. Jia, A. Migliore, N. Xin, S. Y. Huang, J. Y. Wang, Q. Yang, S. P. Wang, H. L. Chen, D. M. Wang, B. Y. Feng, Z. R. Liu, G. Y. Zhang, D. H. Qu, H. Tian, M. A. Ratner, H. Q. Xu, A. Nitzan and X. F. Guo, *Science*, 2016, **352**, 1443.
19 D. Kim, H. Jeong, H. Lee, W. T. Hwang, J. Wolf, E. Scheer, T. Huhn, H. Jeong and T. Lee, *Adv. Mater.*, 2014, **26**, 3968.
20 J. Chen, W. Wang, M. A. Reed, A. M. Rawlett, D. W. Price and J. M. Tour, *Appl. Phys. Lett.*, 2000, **77**, 1224.
21 S. Park and H. J. Yoon, *Nano Lett.*, 2018, **18**, 7715.
22 A. Tan, J. Balachandran, S. Sadat, V. Gavini, B. D. Dunietz, S.-Y. Jang and P. Reddy, *J. Am. Chem. Soc.*, 2011, **133**, 8838.
23 L. Cui, R. Miao, K. Wang, D. Thompson, L. A. Zotti, J. C. Cuevas, E. Meyhofer and P. Reddy, *Nat. Nanotechnol.*, 2018, **13**, 122.
24 W. Du, T. Wang, H.-S. Chu, L. Wu, R. Liu, S. Sun, W. K. Phua, L. Wang, N. Tomczak and C. A. Nijhuis, *Nat. Photonics*, 2016, **10**, 274.
25 G. D. Kong and H. J. Yoon, *J. Electrochem. Soc.*, 2016, **163**, G115.
26 Y. Li, J. Huang, R. T. McIver Jr. and J. C. Hemminger, *J. Am. Chem. Soc.*, 1992, **114**, 2428.
27 M. H. Schoenfisch and J. E. Pemberton, *J. Am. Chem. Soc.*, 1998, **120**, 4502.
28 C. M. Crudden, J. H. Horton, I. I. Ebralidze, O. V. Zenkina, A. B. McLean, B. Drevniok, Z. She, H.-B. Kraatz, N. J. Mosey, T. Seki, E. C. Keske, J. D. Leake, A. Rousina-Webb and G. Wu, *Nat. Chem.*, 2014, **6**, 409.
29 E. A. Doud, M. S. Inkpen, G. Lovat, E. Montes, D. W. Paley, M. L. Steigerwald, H. Vázquez, L. Venkataraman and X. Roy, *J. Am. Chem. Soc.*, 2018, **140**, 8944.
30 E. A. Weiss, G. K. Kaufman, J. K. Kriebel, Z. Li, R. Schalek and G. M. Whitesides, *Langmuir*, 2007, **23**, 9686.
31 R. C. Chiechi, E. A. Weiss, M. D. Dickey and G. M. Whitesides, *Angew. Chem., Int. Ed.*, 2008, **47**, 142.
32 J. G. Simmons, *J. Appl. Phys.*, 1963, **34**, 2581.
33 C. M. Crudden, J. H. Horton, M. R. Narouz, Z. Li, C. A. Smith, K. Munro, C. J. Baddeley, C. R. Larrea, B. Drevniok, B. Thanabalasingam, A. B. McLean, O. V. Zenkina, I. I. Ebralidze, Z. She, H.-B. Kraatz, N. J. Mosey, L. N. Saunders and A. Yagi, *Nat. Commun.*, 2016, **7**, 12654.
34 G. Lovat, E. A. Doud, D. Lu, G. Kladnik, M. S. Inkpen, M. L. Steigerwald, D. Cvetko, M. S. Hybertsen, A. Morgante, X. Roy and L. Venkataraman, *Chem. Sci.*, 2019, **10**, 930.
35 H. K. Kim, A. S. Hyla, P. Winget, H. Li, C. M. Wyss, A. J. Jordan, F. A. Larrain, J. P. Sadighi, C. Fuentes-Hernandez, B. Kippelen, J.-L. Bredas, S. Barlow and S. R. Marder, *Chem. Mater.*, 2017, **29**, 3403–3411.
36 G. D. Kong, M. Kim, S. J. Cho and H. J. Yoon, *Angew. Chem., Int. Ed.*, 2016, **55**, 10307.
37 K. C. Liao, H. J. Yoon, C. M. Bowers, F. C. Simeone and G. M. Whitesides, *Angew. Chem., Int. Ed.*, 2014, **53**, 3889.
38 S. Y. Quek, H. J. Choi, S. G. Louie and J. B. Neaton, *Nano Lett.*, 2009, **9**, 3949.
39 S. E. Byeon, M. Kim and H. J. Yoon, *ACS Appl. Mater. Interfaces*, 2017, **9**, 40556.
40 P. Reddy, S.-Y. Jang, R. A. Segalman and A. Majumdar, *Science*, 2007, **315**, 1568.
41 J. A. Malen, P. Doak, K. Baheti, T. D. Tilley, A. Majumdar and R. A. Segalman, *Nano Lett.*, 2009, **9**, 3406.
42 K. Baheti, J. A. Malen, P. Doak, P. Reddy, S.-Y. Jang, T. D. Tilley, A. Majumdar and R. A. Segalman, *Nano Lett.*, 2008, **8**, 715.
43 S. Y. Quek, H. J. Choi, S. G. Louie and J. B. Neaton, *ACS Nano*, 2011, **5**, 551.